Petroleum Research 11 (2026) 431–440

Contents lists available at ScienceDirect

Petroleum Research

journal homepage: http://www.keaipublishing.com/en/journals/petroleum-research/

Full Length Article

# Spatially continuous regularization of the parameters of the capacitance–resistance model

Egor Illarionov [a,b,*], Elizaveta Gladchenko [c], Anton Voskresenskii [a,d], Sergey Safonov [a], Klemens Katterbauer [e]

[a] Aramco Innovations, Moscow, Russia
[b] Moscow State University, Moscow, Russia
[c] Center for Petroleum Science and Engineering, Moscow, Russia
[d] ITMO University, Saint-Petersburg, Russia
[e] Saudi Aramco, Dhahran, Saudi Arabia

ARTICLE INFO

*Article history:*
Received 26 February 2025
Received in revised form
30 August 2025
Accepted 11 September 2025
Available online 19 September 2025

*Keywords:*
Capacitance-resistance model
Machine learning
Neural networks
Petroleum

ABSTRACT

The capacitance–resistance model (CRM) is a widely-used model for predicting well production rates because it requires the estimation of only a small number of parameters to describe production wells and the connectivity between injection and production wells. However, CRM parameters are not inherently spatially constrained, which can lead to unnatural results. In this research, we conducted spatially continuous regularization of CRM parameters and investigated how it affected model accuracy. A related goal was to investigate how this regularization improved the spatial interpolation of CRM coefficients. For regularization, we considered CRM parameters as values for a spatially continuous function, implemented this function using a neural network, and fitted it using production history data. We employed two benchmark datasets—the egg and Costa datasets—to compare two models: the unconstrained conventional CRM and the proposed spatially regularized CRM. We concluded that the spatially regularized CRM yielded accuracy close to that of the conventional CRM; however, it provided a more interpretable spatial distribution of the CRM parameters.



## 1. Introduction

The capacitance–resistance model (CRM) is a simple and useful model for approximating liquid flow rates in hydrocarbon reservoir production wells (Yousefi et al., 2019) based on a material balance equation and an inflow equation (Yousef et al., 2006a; 2006b). The first equation defines the reservoir pressure response to liquid inflow and outflow rates, and the second defines the production well deliverability with respect to reservoir pressure and bottomhole pressure (BHP). Excluding the reservoir pressure, one obtains a closed-form equation, which relates the production rate $q_n(t)$ of the $n$-th well to the BHP $p_n(t)$ of the well and the injection rate $I_k(t)$ of the $k$-th injector. We provide the governing equation in the form used by Gladchenko et al. (2023a), which will be referred to as the conventional CRM:

$$q_n(t) = \widehat{\lambda}_n \exp\left(\frac{-t}{\widehat{\tau}_n}\right)\left[q_n(0) + \int_0^t \exp\left(\frac{s}{\tau_n}\right) \times \left(\frac{1}{\tau_n}\sum_k f_{kn} I_k(s) - J_n \frac{\mathrm{d}p_n(s)}{\mathrm{d}s}\right)\mathrm{d}s\right], \tag{1}$$

where $q_n(t)$ is the liquid rate of the $n$-th production well at time $t$, $I_k(s)$ is the injection rate of the $k$-th injection well at time $s$, $\widehat{\lambda}_n$ is the correction parameter of the $n$-th production well, $\widehat{\tau}_n$ is the primary depletion rate of the $n$-th production well, $\tau_n$ is the depletion rate of the $n$-th production well, $f_{kn}$ is the connectivity coefficient that defines the influence of the $k$-th injection well on the $n$-th production well, $J_n$ is the productivity index of the $n$-th production

* Corresponding author. Aramco Innovations, Moscow, Russia.
*E-mail address:* egor.illarionov@math.msu.ru (E. Illarionov).
Peer review under the responsibility of Editorial Office of Petroleum Research.

https://doi.org/10.1016/j.ptlrs.2025.09.001

well, $p_n(s)$ is the BHP of the $n$-th production well at time $s$.

Larger $\hat{\tau}$ and $\tau$ values mean that, at a constant BHP and injection rate, the well production rate decays more slowly; larger $f$ values provide a greater production rate response to a unit change in the injection rate; and larger $J$ values provide a greater production rate response to a unit change in BHP. However, in the conventional CRM, $\hat{\tau}n = \tau_n$, Gladchenko et al. (2023a) found that considering the terms as independent parameters provided a better fit for production data. It is also common to assume that:

$$\sum_n f_{kn} = 1 \tag{2}$$

This means that the $k$-th injection well fully distributes the injected water between the production wells.

The moderate number of parameters and their simple physical interpretation make this model attractive to engineers. However, various CRM modifications have been proposed, for example, for karst reservoirs (Wang et al., 2019), for immiscible gas flooding (Yousefi et al., 2019), for estimating waterflood performance (Chen et al., 2010), for flow barrier detection (Ogali and Orodu, 2022), and for large-scale reservoirs (Aslam et al., 2022). More examples can be found in review papers (Holanda et al., 2018; Sayarpour et al., 2009; Wanderley de Holanda et al., 2018). Recently, Gladchenko et al. (2023b) considered conventional CRM in the context of physics-informed neural networks (PINNs). The idea behind their approach was to train a neural network model that fitted both the differential form of the CRM and observational data. Please see Latrach et al. (2024) for a further review of physics-informed models applied to subsurface simulation. The CRM framework (Eq. (1)) considers wells as a disordered set of producers and injectors and does not account for their spatial positions. On the one hand, this simplifies model fitting (estimation of the model parameters given relevant historical data); on the other, the lack of spatial constraints in practice can lead to unnatural results (e.g., closely located wells require significantly different parameters, and distantly located wells exhibit strong connectivity). To avoid such situations, one could, for example, set a maximal radius within which an injection well can affect production wells, which is considered the simplest approach to spatial regularization. A common case of spatial regularization being important arises when interpolating CRM parameters, such as when applying the CRM to well-placement optimization (see, e.g., Arouri et al. (2022); Gladchenko et al. (2023a)). Interpolation seems reasonable when the data are sufficiently smooth; however, CRM parameters are not inherently constrained to spatial smoothness, so their interpolation can lead to unrealistic results.

The aim of our research was to explicitly supplement the CRM with spatial information about well locations and to optimize the CRM parameters with constraints according to this spatial information. We replaced the discrete set of CRM parameters with spatially continuous functions implemented using neural networks and optimized these functions using historical production rates. This approach ensured the spatial continuity of the CRM parameters and did not require additional models for interpolation. The next section provides the mathematical details of this approach.

## 2. A spatially regularized capacitance–resistance model

The main idea underpinning our approach was to consider the CRM parameters in Eq. (1) as the values of a spatially continuous function evaluated at the locations of the corresponding wells. Indeed, the parameters $\hat{\lambda}_n$, $\hat{\tau}_n$, $\tau_n$, and $J_n$ depend on the coordinates $\vec{r}_n = (x_n, y_n)$ of production well. Thus, we assumed that functions $\hat{\lambda}(\vec{r})$, $\hat{\tau}(\vec{r})$, $\tau(\vec{r})$, and $J(\vec{r})$ existed, such that for the $n$-th production well, located at $\vec{r}_n = (x_n, y_n)$, we had $\hat{\lambda}_n = \hat{\lambda}(\vec{r}_n)$, $\hat{\tau}_n = \hat{\tau}(\vec{r}_n)$, $\tau n = \tau(\vec{r}_n)$, and $J_n = J(\vec{r}_n)$. The $fkn$ parameters (connectivity coefficients) are particularly delicate because they represent the relationships between pairs of wells and thus depend on pairs of coordinates for the locations of the injection well and the production well. Without losing generality, one can assume that a function $f(\vec{r}, \vec{r}')$ exists, such that $f_{kn} = f(\vec{r}_k, \vec{r}_n)$, where $\vec{r}_k$ is the location of the $k$-th injection well and $\vec{r}_n$ is the location of the $n$-th production well. Eq. (1) now reads:

$$q_n(t) = \hat{\lambda}\left(\vec{r}_n\right)\exp\left(\frac{-t}{\hat{\tau}\left(\vec{r}_n\right)}\right)\left[q_n(0) + \int_0^t \exp\left(\frac{s}{\tau\left(\vec{r}_n\right)}\right)\right.$$
$$\left.\times\left(\frac{1}{\tau\left(\vec{r}_n\right)}\sum_k f\left(\vec{r}_k, \vec{r}_n\right)I_k(s) - J\left(\vec{r}_n\right)\frac{\mathrm{d}p_n(s)}{\mathrm{d}s}\right)\mathrm{d}s\right], \tag{3}$$

where $\vec{r}_n = (x_n, y_n)$ is the coordinate of the $n$-th production well, and $\vec{r}_k = (x_k, y_k)$ inside the sum sign enumerates the injection wells. We refer to the model given by Eq. (3) as SpatialCRM.

To ensure the continuity of spatial functions and automate their estimation, we used neural networks, the inputs of which were the spatial coordinates $(x, y)$. This is illustrated in Fig. 1.

Neural networks, by design, are continuous functions, and varying their architectures (i.e., the number of hidden layers and the number of neurons) allows more or less complex dependencies to be modeled. Thus, the use of neural networks not only facilitates spatially continuous regularization but also controls the variability of spatial functions. In more detail, we represented the functions $\hat{\lambda}(\vec{r})$, $\hat{\tau}(\vec{r})$, $\tau(\vec{r})$, and $J(\vec{r})$ using separate fully connected neural networks, each with two inputs $(x, y)$, several hidden layers, and one output. For the hidden and output layers, we used the activation function $SoftPlus(x) = \ln(1 + \exp(x))$ to ensure, in particular, that the output was always nonnegative (see Szandała [2021] for a review of activation functions). In the conventional CRM, the connectivity parameters are constrained by Eq. (2); hence, the function $f(\cdot, \cdot)$ values are also constrained. To simplify the further analysis, we considered the unconstrained

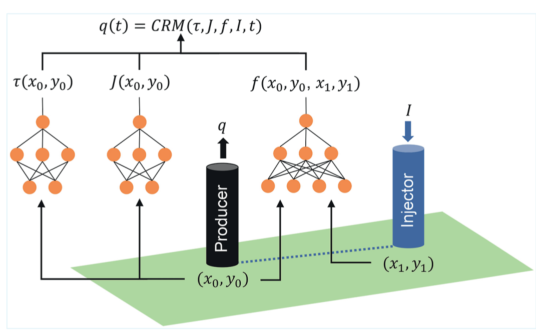


**Fig. 1.** Illustration of the spatially regularized CRM: The model parameters $\tau$ and $J$ are considered functions of the production well coordinates $(x_0, y_0)$, and the strength of connectivity between the injection and producer is assumed to be a function $f$ of the coordinates of both wells, $(x_0, y_0)$ and $(x_1, y_1)$. Orange circles represent the fully connected neural network models used to approximate these functions. When these parameters are evaluated, the production liquid rate $q(t)$ is computed according to the conventional CRM equation.

function $\tilde{f}(\vec{r}, \vec{r}')$ and related it to the connectivity coefficients $f_{kn}$ using normalization:

$$f_{kn} = \tilde{f}\left(\vec{r}_k, \vec{r}_n\right) \bigg/ \sum_m \tilde{f}\left(\vec{r}_k, \vec{r}_m\right), \tag{4}$$

where $\vec{r}_k$ is the location of the $k$-th injection well, $\vec{r}_n$ is the location of the $n$-th production well, and summation is across all positions $\vec{r}_m$ of production wells.

The function $\widehat{f}$ defining the (nonnormalized) connectivity coefficients can be additionally regularized in differentways, such as:

- $\tilde{f} = \tilde{f}(\vec{r}, \vec{r}')$, meaning that connectivity explicitly depends on the locations of the injection and production wells (no regularization)
- $\tilde{f} = \tilde{f}(\vec{r}, \|\vec{r} - \vec{r}'\|)$, meaning that the connectivity depends on the location of the injection well and the distance to the production well (isotropic regularization)
- $\tilde{f} = \tilde{f}(\|\vec{r} - \vec{r}'\|)$, meaning that connectivity depends only on the distance between the injection and production wells (isotropic and homogeneous regularization)

In each case, we implemented the function $\tilde{f}$ using a fully connected neural network model with the corresponding number of inputs and one output. We used the same SoftPlus activation function for the hidden and output layers to ensure that the output (the connectivity coefficient) was always nonnegative. Herein, we specify the kind of regularization we used for the reservoir model in each test case. For the numerical approximation of Eq. (3), we approximated the time integral using the finite sum over the time steps used in the reservoir model simulation. For implementation, we used a framework (specifically, PyTorch) that permitted automatic differentiation (Paszke et al., 2019). For neural network training, we used the standard loss function for CRM optimization:

$$loss = \sum_{i,n} (\widehat{q}_n(t_i) - q_n(t_i))^2, \tag{5}$$

where $\widehat{q}_n(t_i)$ is the liquid flow rate predicted using Eq. (3), $q$ is the historical rate, and the sum is across all production wells and time steps for which historical rates are available. At each training step, we computed the loss value (5) and updated the weights of the neural network models using the Adam optimization algorithm (Kingma and Ba, 2014). We repeated the training steps until the loss no longer decreased significantly.

It should be noted that the number of neurons in the hidden layer played an important role in the model training process. In fact, it provided additional model regularization. A large number of neurons made the parameters of the wells spatially independent. In contrast, a small number of neurons increased the spatial correlation between the wells and forced the model to find a balance between rate fitting and the smoothness of the spatial distribution of the well parameters. The same reasoning could be applied to the depth (the number of hidden layers) of the neural network model. To improve the convergence of the training process, we found it useful to scale the coordinates of the wells to a unit range and normalize the BHP, production, and injection rates to unit mean.

## 3. Results

Two benchmark reservoir models were considered in this study. The first contains a small number of wells, and one well is introduced with a time delay relative to the other wells. Here, we evaluate the interpolation capabilities of both CRM versions. The second case contains a large number of production and injection wells, which usually causes difficulties for the conventional CRM. We combined the descriptions of the reservoir models and experimental results to condense the text.

### 3.1. Egg benchmark

We started experiments using the dataset associated with the open-source synthetic reservoir model named the egg dataset (Jansen et al., 2014). This dataset contains 100 realizations of a channelized oil reservoir with different channel locations. Due to the heterogeneous distribution of geologic parameters, we found this recently published model benchmark more interesting for evaluation than, for example, the SPE model 2 benchmark, which was previously widely used. Each model in the egg dataset comprises a grid of size $60 \times 60 \times 7 = 25{,}200$ cells, 18,553 of which are active. We chose one of the realizations and proceeded with the given locations of four production and eight injection wells. Fig. 2 shows the selected model. The original model prescribed a constant 296-bar BHP for each production well, which was not very helpful for CRM validation. We resampled the BHP, varying it randomly with a probability of 1/3 each month between 285 and 296 bars for the 2010–2020 period. Fig. 3 shows the obtained schedule for the PROD1 and PROD2 wells.

The last change we made to the default model was to reduce the permeability by multiplying the given permeability by 0.01. We did this because, using the initial values, we observed a rapid drop in oil flow rates and an increase in water rates after the simulation. Reducing permeability helped us avoid this nonstationarity. Using this benchmark model, we first compared the accuracy of the two versions of CRM for each well in detail. Then we placed a new well in the reservoir that started production with a delay (i.e., later than the initial wells) and compared the interpolation accuracy of the CRM versions. More precisely, we placed the new well between the PROD1 and PROD3 wells. The new well started to operate in 2018, and we generated the BHP schedule as described previously. The reason for placing a new well at this specific location was twofold. First, we sought to identify the point with the highest oil saturation in 2018. Second, we could not place

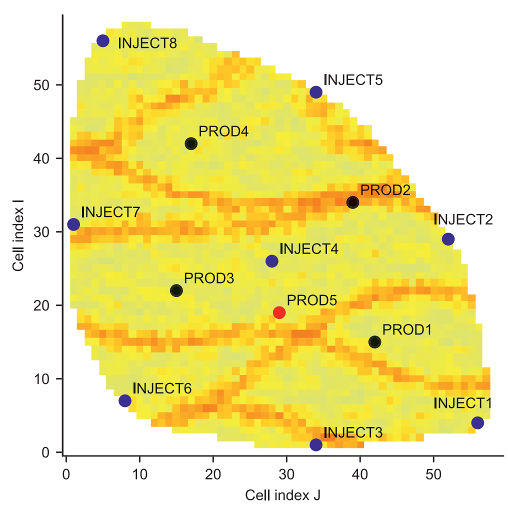


**Fig. 2.** Distribution of x-permeability in the top layer of the egg reservoir model and the location of the production and injection wells. The PROD5 well is the new well introduced in this article.

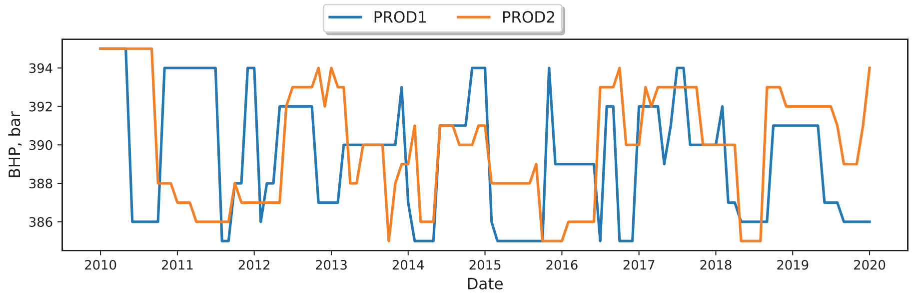


**Fig. 3.** Bottomhole pressure (BHP) generated for the PROD1 and PROD2 production wells.

the well outside the convex hull of existing wells, since we would then have had to extrapolate the CRM coefficients rather than interpolate them.

We used a commercial simulator (tNavigator) to simulate the compiled reservoir model and obtain production and injection rates to train and evaluate both versions of CRM. More specifically, we used the 2010–2016 period to train the model, 2016–2018 to evaluate the model accuracy for a set of existing wells, and 2018–2020 to investigate the model performance when the new well was introduced. Given the results of the simulation model for production liquid rates, bottom-hole pressures, and injection rates, we trained both versions of CRM using the 2010–2016 period only. Specifically, we used the following neural network architectures in SpatialCRM:

- fully connected models with a 2–10–1 sequence of neurons for the functions $\widehat{\lambda}(\overrightarrow{r})$, $\widehat{\tau}(\overrightarrow{r})$, $\tau(\overrightarrow{r})$, and $J(\overrightarrow{r})$

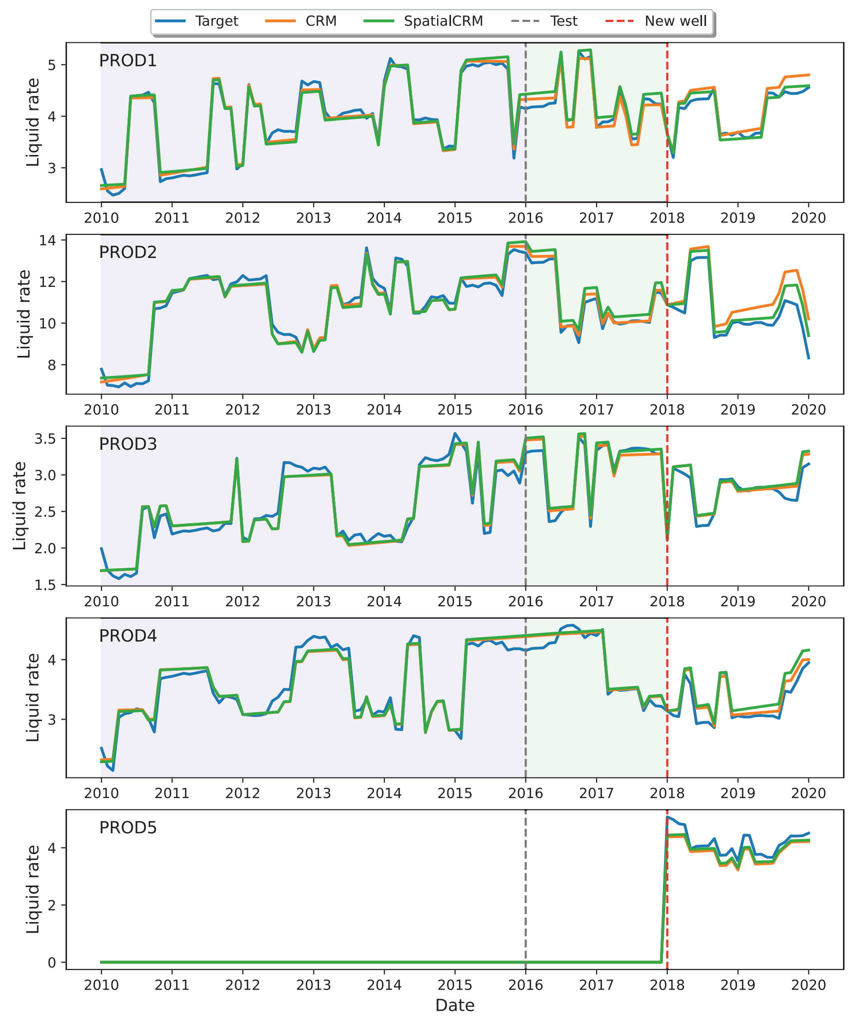


**Fig. 4.** Target (ground truth) liquid rates (blue lines) predicted using the conventional CRM (orange line) and SpatialCRM (green line). The blue background indicates the period used for model training, the green background shows the testing period, and the white background shows the period when the new well (PROD5) was introduced.

**Table 1**
MAPE metrics (as percentages) for the egg dataset. The training period is 2010–2016, the testing period is 2016–2018, and the forecast period is 2018–2020. The left value in each cell is the MAPE metric for the conventional CRM, and the right value is for SpatialCRM.

| Well | Train | Test | Forecast |
|---|---|---|---|
| PROD1 | 2.4 \| 2.8 | 2.5 \| 3.2 | 3.5 \| 2.2 |
| PROD2 | 2.2 \| 2.5 | 1.4 \| 3.9 | 2.2 \| 3.8 |
| PROD3 | 3.6 \| 3.6 | 2.6 \| 2.7 | 2.8 \| 2.8 |
| PROD4 | 2.8 \| 2.8 | 2.4 \| 2.6 | 2.8 \| 2.6 |
| PROD5 | – \| – | – \| – | 7.6 \| 5.3 |
| Average | 2.7 \| 2.9 | 2.2 \| 3.1 | 3.8 \| 3.3 |

- a fully connected model with a 4–10–10–1 sequence of neurons for the function $\tilde{f}(\vec{r}, \vec{r}')$

Fig. 4 shows that both models were almost equally accurate in estimating the ground truth production rates (denoted as “target” in the figure) during the training and testing periods for the wells PROD1–PROD4.

For numerical comparison of the predicted and ground truth rates, we used the mean absolute percentage error (MAPE), defined as follows:

$$MAPE = 100\% \times \frac{1}{n}\sum_{i=1}^{n}\left|\frac{\hat{q}_i - q_i}{q_i}\right| \tag{6}$$

where $q_i$ is the ground truth value (liquid flow rate), $\hat{q}_i$ is the prediction, and $n$ is the number of samples. Table 1 shows the MAPE metrics for each well for both models.

In 2018, a new well was introduced. To obtain a prediction for 2018–2020, we proceeded as follows. For the conventional CRM, we interpolated the CRM coefficients using ordinary kriging, as described by Gladchenko et al. (2023a). The application of ordinary kriging involves first estimating the mean field value and the variogram, which are then used to compute the coefficients in a linear combination of known values that give the estimate for the new point. It should be noted that these steps include a number of hyperparameters that are usually adjusted by geologists to obtain the most representative results. For SpatialCRM, we used the obtained spatial functions to derive CRM coefficients for the location of the new well. In both cases, we normalized the connectivity coefficients following Eq. 4.

Fig. 5 shows the obtained spatial distributions of the $\tau$ and $J$ coefficients. We observed that both models yielded comparable patterns, meaning that in this case, SpatialCRM was equivalent in composition to the conventional CRM and ordinary kriging models. Moreover, SpatialCRM did not require an intermediate variogram estimation step and thus acted as an end-to-end solution. We also observed that the spatial CRM provided more reasonable extrapolation of the $\tau$ and $J$ coefficients, whereas the ordinary kriging model yielded negative values in some areas (note that ordinary kriging is not inherently constrained to a positive domain). Fig. 6 shows the connectivity matrices obtained using both approaches. In SpatialCRM, connectivity coefficients are the values of the function $\tilde{f}$ calculated at the location of a pair of wells. We observed that the connectivity matrices became rather similar and reasonable with respect to the actual well locations and geological structures.

To predict the liquid flow rate after 2018 (the date when we introduced the new PROD5 well), we assumed that at the time the new well started production, the initial liquid flow rate of the new well and the instantaneous liquid flow rates of the existing wells were known. Thus, to obtain a prediction for the PROD5 well, we applied the CRM equation using the new coefficients and the value of the start rate. In the case of existing wells (PROD1–PROD4), we continued the previous calculation with a start date of 2010, but we used new coefficients for the 2018–2020

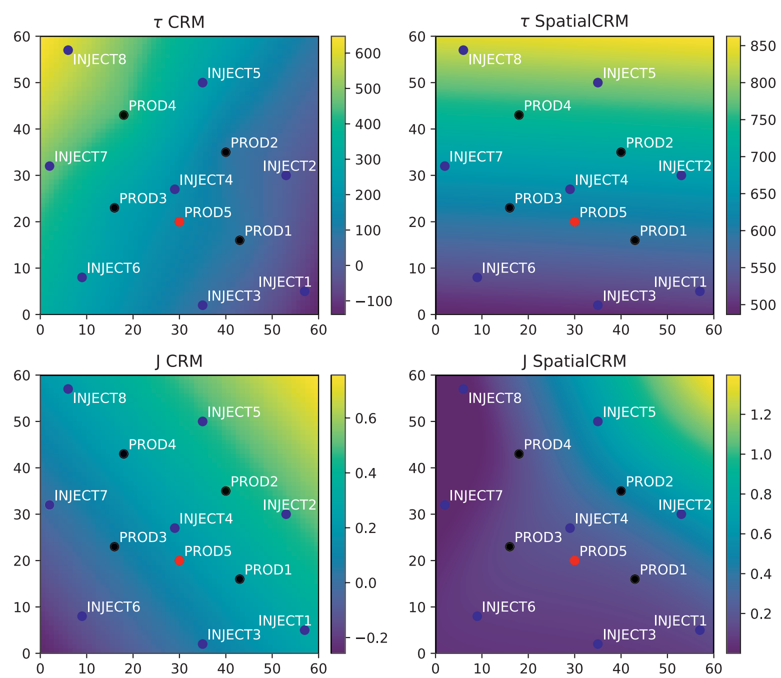


**Fig. 5.** Spatial distribution of parameters $\tau$ and $J$. The left column was obtained by kriging the corresponding well parameters estimated using the conventional CRM. The right column was obtained directly by computing the spatial functions in SpatialCRM.

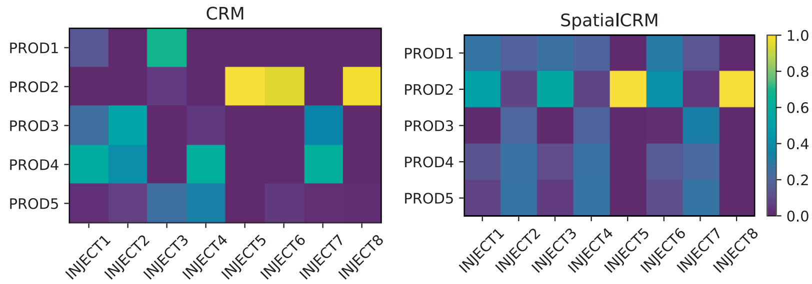


**Fig. 6.** Left panel: matrix constructed from connectivity coefficients ($f_{kn}$) estimated using the conventional CRM (index $k$ corresponds to the injection wells or columns of the matrix, and index $n$ – corresponds to the production wells or rows of the matrix). Right panel: matrix constructed from the normalized values of the spatial function $\tilde{f}(\overrightarrow{r}, \overrightarrow{r}')$ estimated using SpatialCRM and calculated at the location of the $k$-th injection well and $n$-th production well.

period and applied a constant shift to each well to compensate for the error caused by the introduction of the new PROD5 well. The resulting rates are shown in Fig. 4, and the MAPE metrics are provided in Table 1.

We observed that the connectivity coefficients updated on January 1, 2018, provided a close match to the target production rates for the existing wells and the new well. Now, we summarize the results of the egg benchmark model. We found the following:

- Both approaches provided almost similar results for the estimation of production liquid flow rates before 2018 (training and testing periods), with an average MAPE accuracy of about 3 %.
- The spatial distribution obtained by applying ordinary kriging to the CRM and SpatialCRM coefficients appeared highly consistent. However, ordinary kriging can produce negative (nonphysical) values because it is not inherently constrained to give the positive values expected for well parameters.
- Numerically, both approaches yielded similar predicted production liquid flow rates for the new well introduced in 2018 and for the existing wells after 2018, also with an average MAPE of about 3 %.

### 3.2. Costa benchmark

To conduct a numerical investigation that mimicked real-world data, we used the recently released challenging and realistic benchmark Costa dataset (Gomes et al., 2022), which, among diverse geological and petrophysical data, contains simulated production data for 248 production and 182 water injection wells. Note that the reservoir model used for the production rate simulation remained undisclosed in the Costa dataset for the purposes of this benchmark. We used only a small portion of the original data that represented simulated well liquid production and injection rates, bottom-hole pressures, and well coordinates. Additionally, we focused on the 2040–2050 period, during which the number of wells remained constant. Fig. 7 shows the locations of the production and injection wells and an example of well production rates and bottom-hole pressures.

We split the 2040–2050 period into two parts to train the models (2040–2048) and to evaluate their performance (2048–2050). To compare the predicted and target rates, we used MAPE metrics averaged across all production wells. Because of the large number of wells, we used deeper neural network architectures:

- fully connected models with a 2–32–64–32–16–8–1 sequence of neurons for $\widehat{\lambda}(\overrightarrow{r})$, $\widehat{\tau}(\overrightarrow{r})$, $\tau(\overrightarrow{r})$, and $J(\overrightarrow{r})$
- fully connected model with a 3–64–32–1 sequence of neurons for the function $\tilde{f}(\overrightarrow{r}, \|\overrightarrow{r} - \overrightarrow{r}'\|)$

Fig. 8 shows the results for the conventional CRM and SpatialCRM training and predictions during the testing period for several wells. The distribution of MAPE metrics across all production wells during the testing period is shown in Fig. 9. We

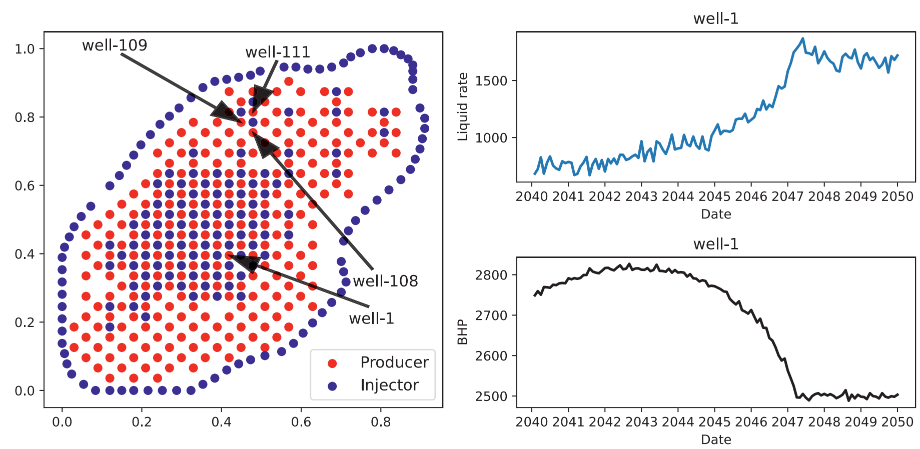


**Fig. 7.** The left panel shows the location of production (red dots) and injection (blue dots) wells in the Costa benchmark model. The right panel shows the production rates and bottom-hole pressure for a sample production well. Arrows indicate wells used here and in the next plots for illustration of production rates.

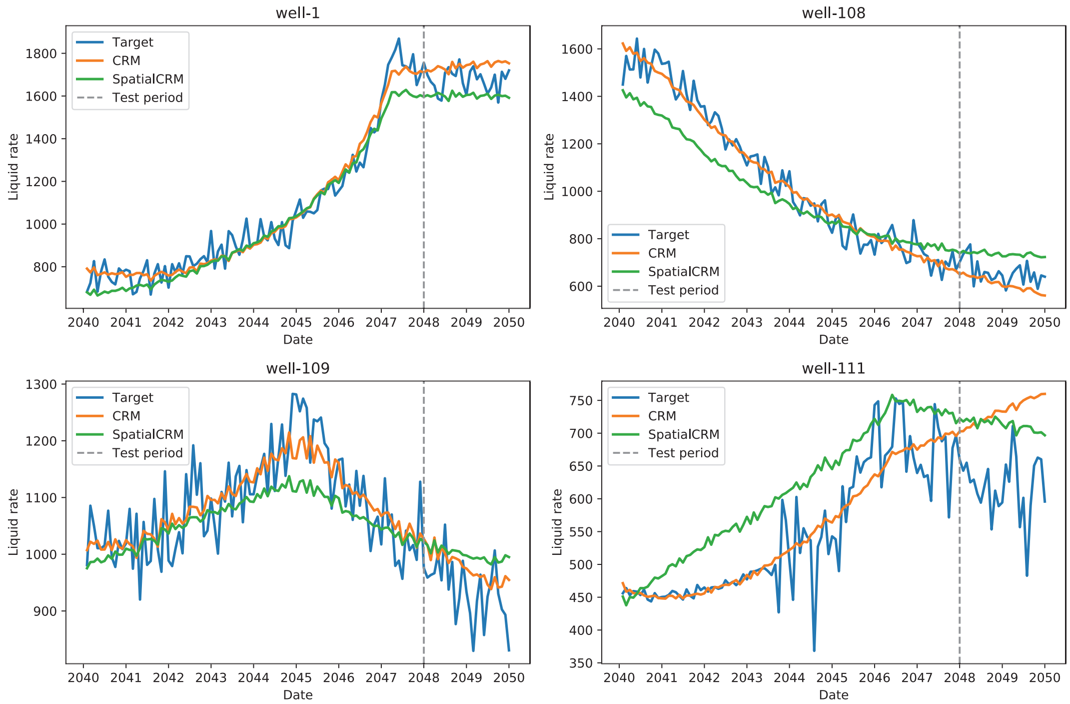


**Fig. 8.** Comparison of the target (ground truth) liquid flow rates (blue line) with the predictions obtained using the conventional CRM (orange line) and SpatialCRM (green line). The selected wells exhibited different rate patterns in the Costa dataset.

observed that both models yielded quite a uniform distribution of errors, and the wells that caused large errors for the conventional CRM were also challenging for SpatialCRM. We expected this because both models relied on the same physical equation. On average, we obtained MAPE metrics for training and test subsets equal to 4.1 % and 10.2 % for the conventional CRM and 8.0 % and 13.6 % for SpatialCRM. Somewhat larger errors were also expected because SpatialCRM solves the constrained problem in contrast to the conventional CRM.

However, we argue that the cost of the slightly higher accuracy of the conventional CRM is unrealistic connectivity coefficients. Indeed, Fig. 10 shows that the connectivity coefficients obtained using the conventional CRM became almost independent of an injection well (i.e., injection wells have connectivity similar to production wells). In particular, this implied that all injected wells could be joined into a single virtual injector that would distribute all the injected water between production wells. Although this may have allowed for a good match with the production values, this pattern did not seem realistic and was not reasonable for interpolation. In contrast, due to the prior spatial constraint, we observed more localized connectivity using SpatialCRM.

Fig. 11 demonstrates the distribution of $\tau$ and $J$ parameters across production wells for both versions of the CRM. We observed that the parameters obtained using the conventional CRM approach varied greatly locally, whereas the parameters obtained using SpatialCRM were smooth and locally consistent. Moreover, the large-scale patterns for both distributions were similar. For example, the central region of the reservoir had lower values for the $\tau$ parameter in both cases. Additionally, the $J$ parameter was higher in the central part of the reservoir model in both cases. We concluded that for these parameters, both approaches were rather consistent at large spatial scales, but they exhibited significant differences at small scales, which may be important for the interpolation of CRM parameters, among others.

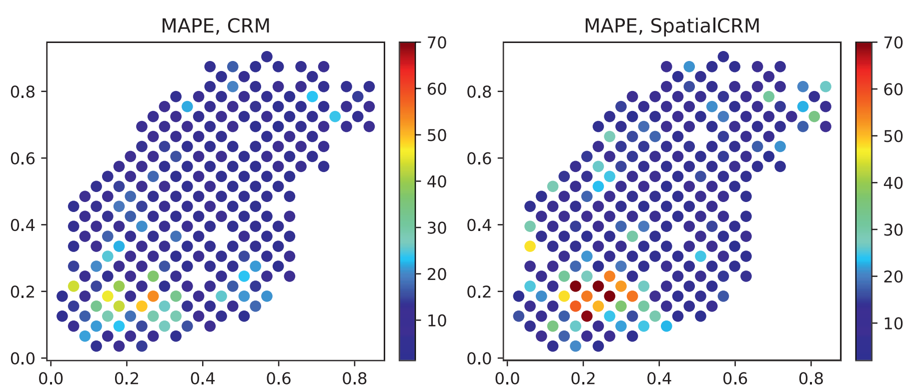


**Fig. 9.** Distribution of MAPE metrics across production wells during the testing period for the conventional CRM (left panel) and SpatialCRM (right panel).

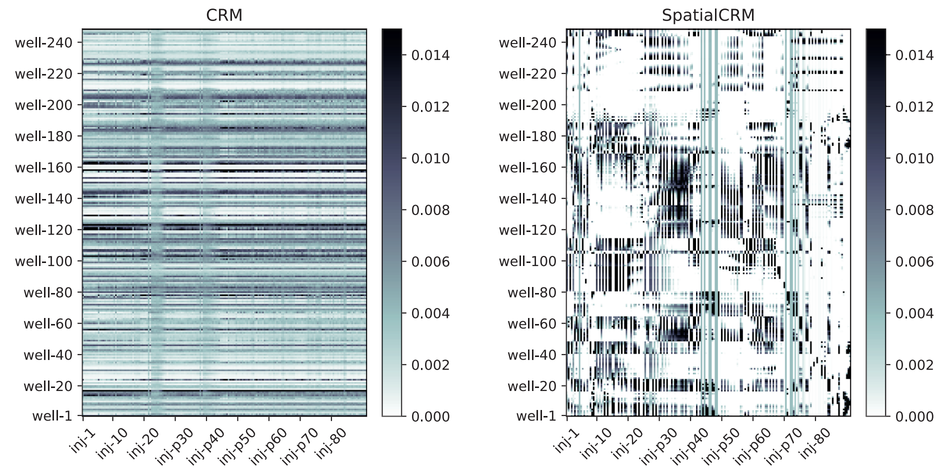


**Fig. 10.** Connectivity matrix between production (vertical axis) and injection (horizontal axis) wells. The left panel is for the conventional CRM and contains CRM parameters, $f_{kn}$, and the right panel is for SpatialCRM, constructed from the normalized values of the spatial function $\tilde{f}(\vec{r}, \|\vec{r} - \vec{r}'\|)$ estimated using SpatialCRM and calculated at the locations of the $k$-th injection and $n$-th production wells.

Finally, for each injection well, we created a connectivity map by estimating the connectivity coefficient between each point in the reservoir domain and the injection well. As previously mentioned, for the conventional CRM, we applied ordinary kriging, whereas for SpatialCRM, we used the function $\tilde{f}$ to compute the connectivity between two given points. Consequently, we obtained 182 maps (according to the number of injection wells), with each map describing the spatial influence of each injector (note that, for the conventional CRM, all these maps became similar according to Fig. 10, whereas they differed for SpatialCRM). For visualization, we averaged these maps and plotted them in Fig. 12. We observed that the map obtained using kriging was more locally inhomogeneous and noisy (as expected for kriging). In contrast, the map obtained using SpatialCRM appeared smoother. Both maps indicated greater influence of injectors in the central part of the reservoir model, which seemed reasonable. We derived values

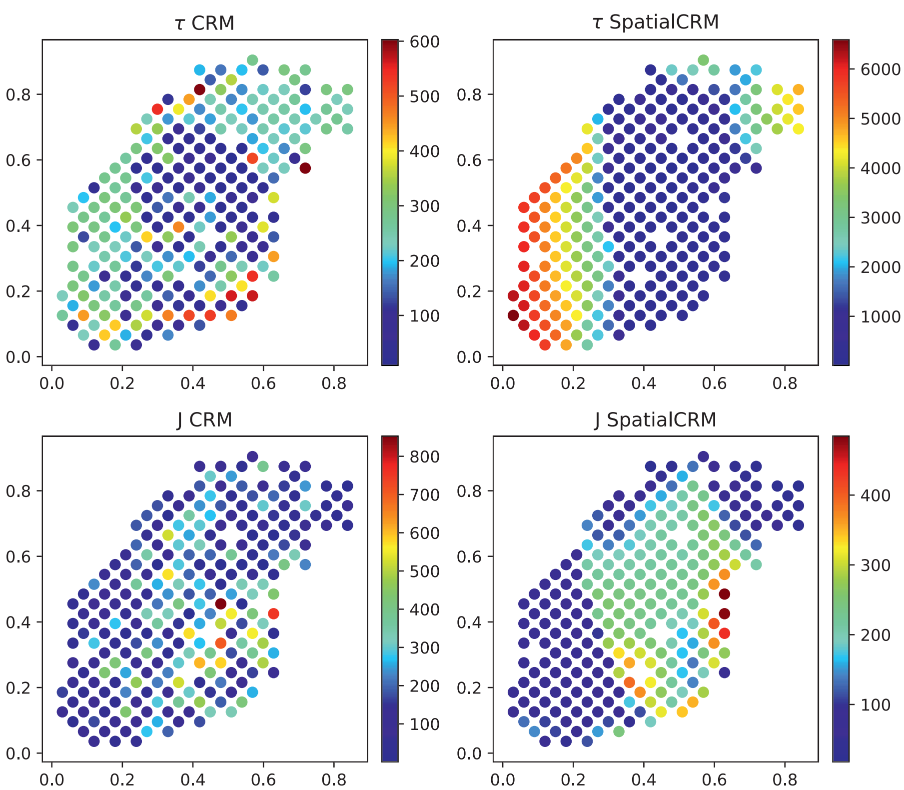


**Fig. 11.** Distribution of parameters $\tau$ and $J$ across production wells. The left column is for the conventional CRM, and the right columns are for SpatialCRM.

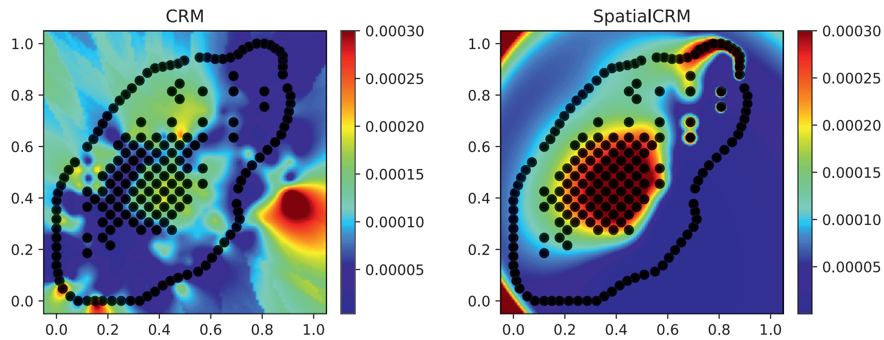


**Fig. 12.** Average influence of all injectors at each point in the reservoir region. The values in the left panel are obtained using kriging applied to the connectivity coefficients for the conventional CRM. The values in the right panel are obtained using SpatialCRM.

outside the injection well area from extrapolation, and they should not be considered representative.

The key results for the Costa benchmark model were summarized. Both approaches provided reasonable estimates of production liquid flow rates, with a MAPE accuracy of about 10 %, but due to the absence of spatial constraints, the conventional CRM produced slightly better results. Simultaneously, we observed that the connectivity coefficients for the conventional CRM appeared unrealistic (all injection wells had similar water distribution patterns between production wells, and the connectivity coefficient for SpatialCRM seemed more localized). The estimated well parameters $\tau$ and $J$ were highly variable locally for the conventional CRM and appeared as smooth fields for SpatialCRM; however, on a large scale, both approaches yielded rather compatible distributions of these parameters.

## 4. Conclusion

We developed a CRM modification to account for the spatial positions of production and injection wells operating with spatially continuous functions instead of discrete sets of parameters, as in the conventional CRM. We implemented spatial functions using fully connected neural network models and well coordinates as inputs. This ensured the continuity of the CRM parameters with respect to the well coordinates and quick optimization of the model using modern computational frameworks. Compared to the conventional CRM, the only additional data required were well coordinates.

To evaluate this approach, we used two benchmark datasets. The first was based on the synthetic egg reservoir model and contained a small number of wells. When the number of wells was small, the influence of spatial constraints was minor. Indeed, we observed that, qualitatively and quantitatively, the two approaches yielded similar predictions. This fact demonstrates that one can set up a constrained (regularized) CRM problem and expect similarly accurate production rate predictions together with spatially smooth CRM parameters. Moreover, the spatial distribution of the CRM parameters obtained using kriging appeared similar to the spatial functions learned by SpatialCRM. Although ordinary kriging includes a number of nontrivial intermediate steps (e.g., the construction of variograms), SpatialCRM acts as an end-to-end solution (from historical data to interpolation) without additional intermediate steps and models).

We then considered the Costa dataset, which is challenging to accurately predict liquid flor rates due to the large number of injection and production wells. The unconstrained conventional CRM provided a more accurate approximation; however, the CRM parameters varied considerably for closely located wells. Moreover, almost all injection wells exhibited similar connectivity patterns, which is unrealistic. In contrast, SpatialCRM yielded smooth fields of CRM parameters and localized connectivity. However, this constraint slightly affected the accuracy of the production rate estimation.

With this research, we continue a discussion regarding what is more important: accuracy in fitting historical data or the physical realism of model parameters. The answer may not be obvious and may depend on the particular application. However, we propose a method that permits a balance between these two points of view. It is also worth noting that when the complexity of the neural network models implementing using spatial functions increased, the role of regularization vanished, and SpatialCRM became equivalent to the conventional CRM.

The Costa benchmark represents a change from a fully synthetic case to data that mimics real-world fields. Since both the conventional CRM and SpatialCRM are based on the same physical equation, the ability to reproduce real-world data primarily depends on matching the assumptions of the physical model to the conditions in an actual reservoir. Since the latter question has been thoroughly discussed in the literature, we did not consider it in this research. Instead, we argue that, among many sets of CRM parameters that can yield high accuracy, additional regularization based on the spatial smoothness of parameters may be more useful for obtaining a realistic set of well parameters.

The proposed spatial regularization of CRM parameters may be particularly appropriate when these parameters have to be interpolated. The point is that interpolation seems reasonable for smooth data; however, the conventional CRM does not ensure it. Our approach solves both problems at once; it controls the spatial variability of CRM parameters and interpolates them in the spatial domain. Note that the values for spatial functions outside the production well region (i.e., extrapolation of CRM parameters) are not assumed to be representative, and we do not discuss their application.

Finally, the proposed implementation of CRM parameters in terms of neural network models, combined with the fact that neural network models permit gradient computation, simplifies the imposition of various physics-based constraints on CRM parameters in the form, for example, of differential equations, as in the framework of physics-informed neural networks.

### CRediT authorship contribution statement

**Egor Illarionov:** Writing – original draft, Methodology, Conceptualization. **Elizaveta Gladchenko:** Investigation, Formal analysis, Data curation. **Anton Voskresenskii:** Methodology.

**Sergey Safonov:** Validation, Resources. **Klemens Katterbauer:** Project administration.

## Data availability statement

The egg reservoir model is available as supplementary data for the article written by Jansen et al. (2014). The COSTA production data are available as supplementary data for the article written by Gomes et al. (2022).

## Declaration of competing interest

The authors declare no competing interests.

## Nomenclature

The notations used in this paper are summarized below:

| | |
|---|---|
| $q_n(t)$ | liquid rate of the $n$-th production well at time $t$ |
| $I_k(s)$ | injection rate of the $k$-th injection well at time $s$ (CRM parameter) |
| $\widehat{\lambda}_n$ | correction parameter for the $n$-th production well (CRM parameter) |
| $\widehat{\tau}_n$ | primary depletion rate for the $n$-th production well (CRM parameter) |
| $\tau_n$ | depletion rate for the $n$-th production well (CRM parameter) |
| $f_{kn}$ | connectivity coefficient that defines the influence of the $k$-th injection well on the $n$-th production well (CRM parameter) |
| $J_n$ | productivity index of the $n$-th production well (CRM parameter) |
| $p_n(s)$ | BHP of the $n$-th production well at time $s$ |
| $\overrightarrow{r} = (x, y)$ | radius vector indicating the spatial location of the well |
| $\widehat{\lambda}(\overrightarrow{r}), \widehat{\tau}(\overrightarrow{r}), \tau(\overrightarrow{r})$, and $J(\overrightarrow{r})$ | spatial functions that substitute for the corresponding CRM parameters |
| $f(\overrightarrow{r}, \overrightarrow{r}')$ | a spatial function that substitutes for the connectivity coefficient |
| $\tilde{f}(\overrightarrow{r}, \overrightarrow{r}')$ | a nonnormalized spatial function used to derive connectivity coefficients |
| BHP | bottomhole pressure |
| MAPE | mean absolute percentage error |
| PINN | physics-informed neural network |

## References


Arouri, Y., Lake, L.W., Sayyafzadeh, M., 2022. Bilevel optimization of well placement and control settings assisted by capacitance- resistance models. SPE J. 27, 3829–3848. https://doi.org/10.2118/210562-PA.

Aslam, B.M., Nugroho, H., Mahendra, F., Kurnia, R., Marhaendrajana, T., Siregar, S., 2022. Capacitance resistance clustered model for mature peripheral waterflood performance prediction and optimization. J. Earth Energy Eng. 11, 118–129. https://doi.org/10.25299/jeee.2022.10633.

Chen, H., Zhang, Z., Sun, W., Li, K., 2010. Modification of capacitance-resistive model for estimating waterflood performance. In: International Oil and Gas Conference and Exhibition in China, SPE. https://doi.org/10.2118/129783-ms.

Gladchenko, E.S., Gubanova, A.E., Orlov, D.M., Koroteev, D.A., 2023a. Kriging-boosted cr modeling for prompt infill drilling optimization. Petroleum. https://doi.org/10.1016/j.petlm.2023.09.003.

Gladchenko, E.S., Illarionov, E.A., Orlov, D.M., Koroteev, D.A., 2023b. Physics-informed neural networks and capacitance-resistance model: fast and accurate oil and water production forecast using end-to-end architecture. In: SPE Symposium Leveraging Artificial Intelligence to Shape the Future of the Energy Industry. https://doi.org/10.2118/214461-ms.

Gomes, J.C., Geiger, S., Arnold, D., 2022. The design of an open-source carbonate reservoir model. Pet. Geosci. 28, 2021–2067. https://doi.org/10.1144/petgeo2021-067.

Holanda, R.W.d., Gildin, E., Jensen, J.L., Lake, L.W., Kabir, C.S., 2018. A state-of-the-art literature review on capacitance resistance models for reservoir characterization and performance forecasting. Energies 11. https://doi.org/10.3390/en11123368.

Jansen, J., Fonseca, R., Kahrobaei, S., Siraj, M., Essen, van, G., Hof, Van den, P., 2014. The egg model - a geological ensemble for reservoir simulation. Geosci. Data J. 1, 192–195. https://doi.org/10.1002/gdj3.21.

Kingma, D.P., Ba, J., 2014. Adam: A Method for Stochastic Optimization. arXiv e-prints. https://doi.org/10.48550/arXiv.1412.6980.

Latrach, A., Malki, M.L., Morales, M., Mehana, M., Rabiei, M., 2024. A critical review of physics-informed machine learning applications in subsurface energy systems. Geoenergy Sci. Eng. 239, 212938. https://doi.org/10.1016/j.geoen.2024.212938. URL: https://www.sciencedirect.com/science/article/pii/S2949891024003087.

Ogali, O.I.O., Orodu, O.D., 2022. Fault characterization and flow barrier detection using capacitance-resistance model and diagnostic plots. J. Petrol. Sci. Eng. 209, 109817. https://doi.org/10.1016/j.petrol.2021.109817.

Paszke, A., Gross, S., Massa, F., Lerer, A., Bradbury, J., Chanan, G., Killeen, T., Lin, Z., Gimelshein, N., Antiga, L., Desmaison, A., Köpf, A., Yang, E., DeVito, Z., Raison, M., Tejani, A., Chilamkurthy, S., Steiner, B., Fang, L., Bai, J., Chintala, S., 2019. Pytorch: an Imperative Style, High-Performance Deep Learning Library. URL: https://arxiv.org/abs/1912.01703.

Sayarpour, M., Zuluaga, E., Kabir, C., Lake, L.W., 2009. The use of capacitance–resistance models for rapid estimation of waterflood performance and optimization. J. Petrol. Sci. Eng. 69, 227–238. https://doi.org/10.1016/j.petrol.2009.09.006.

Szandała, T., 2021. Review and comparison of commonly used activation functions for deep neural networks. In: Bio-inspired Neurocomputing. Studies In Computational Intelligence, Springer Singapore, Singapore, pp. 203–224. https://doi.org/10.1007/978-981-15-5495-7_11.

Wanderley de Holanda, R., Gildin, E., Jensen, J.L., 2018. A generalized framework for capacitance resistance models and a comparison with streamline allocation factors. J. Petrol. Sci. Eng. 162, 260–282. https://doi.org/10.1016/j.petrol.2017.10.020.

Wang, D., Li, Y., Zhang, J., Wei, C., Jiao, Y., Wang, Q., 2019. Improved crm model for inter-well connectivity estimation and production optimization: case study for karst reservoirs. Energies 12, 816. https://doi.org/10.3390/en12050816.

Yousef, A.A., Gentil, P., Jensen, J.L., Lake, L.W., 2006a. A capacitance model to infer interwell connectivity from production- and injection-rate fluctuations. SPE Reservoir Eval. Eng. 9, 630–646. https://doi.org/10.2118/95322-PA.

Yousef, A.A., Lake, L.W., Jensen, J.L., 2006b. Analysis and interpretation of interwell connectivity from production and injection rate fluctuations using a capacitance model. In: SPE Improved Oil Recovery Conference. https://doi.org/10.2118/99998-MS.

Yousefi, S.H., Rashidi, F., Sharifi, M., Soroush, M., 2019. Prediction of immiscible gas flooding performance: a modified capacitance–resistance model and sensitivity analysis. Pet. Sci. 16, 1086–1104. https://doi.org/10.1007/s12182-019-0342-6.